Journal of Science and Transport Technology
Journal homepage: https://jstt.vn/index.php/en

Landslide detection and susceptibility analysis A case study in Pieng stream catchment, Son La province

Tran Trung Hieu[1,2], Dao Dinh Cham[2*], Pham Van Tien[2], Nguyen Cong Quan[2], Pham Thanh Hai[2], Nguyen Duc Anh[2], Bui Phuong Thao[2], Tran Thi Thuy Van[2], Ngo Quoc Trinh[3], Nguyen Trung Thanh[2], Tran Quoc Cuong[4]

[1]International Environmental Doctoral School, University of Silesia in Katowice, Sosnowiec, Poland

[2]Institute of Earth Sciences, Vietnam Academy of Science and Technology, Hanoi, Vietnam

[3]Geotechnical and Artificial Intelligence research group, University of Transport Technology, Hanoi, Vietnam

[4]Ministry of Science and Technology of Vietnam, Hanoi, Vietnam

Article info
Type of article:
Original research paper

DOI:
https://doi.org/10.58845/jstt.utt.2026.en.6.1.282-299

***Corresponding author:**
Email address:
ddcham@ies.vast.vn

Received: 04/08/2025
Received in Revised Form: 02/10/2025
Accepted: 07/11/2025

Abstract: Landslides are a major natural hazard causing significant property damage and loss of life worldwide. In this study, an enhanced landslide inventory was developed for the Pieng Stream catchment (Son La Province) using Object-Based Image Analysis (OBIA) combined with field surveys. Twelve conditioning factors were used to model landslide susceptibility through four machine learning algorithms: extreme gradient boosting (XGB), random forest (RF), multi-layer perceptron (MLP) and logistic regression (LR). Additionally, model interpretation was supported by SHAP, MDA, and PDP analyses. The results demonstrated a high level of reliability for the OBIA method (TPR = 0.886, TS = 0.602). Among the tested models, the XGB model showed the best performance, achieving an AUC of 0.961, an F1 score of 0.915, and an accuracy of 0.915 on the testing dataset. The two most influential predictors identified were lineament density and aspect. An increase in landslide probability was observed with increasing slope, relative relief, lineament density, river density and aspect (0-150°). A total of 88% of testing landslide points were correctly classified within high to very high susceptibility areas, while areas outside the AOA covered merely 0.79% of the study region, indicating a high level of model applicability.

Keywords: OBIA, landslide detection, susceptibility mapping, machine learning, Pieng stream catchment.

1. Introduction

On August 3, 2017, Nam Pam commune, Muong La district, Son La province, experienced severe landslides and debris flows, particularly in the basins of Nam Pam and Pieng streams. These events caused extensive damage to both people and property, resulting in 2 missing persons, 15 injuries, 159 partially damaged houses, and the displacement of 140 households. While several studies on landslide hazards have been conducted in the area, most have focused on small-scale landslide inventories. Therefore, it is essential to

develop a comprehensive landslide inventory, create a detailed landslide susceptibility map, and assess the relative importance of conditioning factors.

Remote sensing is a vital tool in geohazard research, facilitating the assessment and prediction of hazards, particularly in areas that are inaccessible to humans. The advancement of remote sensing technologies, e.g., aerial and high-resolution satellite imagery, has significantly enhanced the interpretation of landslides. Various methods, including traditional, automatic, and semi-automatic approaches, have contributed to these advancements. Barlow [1] developed landslide prediction features using object-based image analysis (OBIA) by incorporating structural features (slope, topography), spectral reflectance, vegetation, slope morphology, river systems, and man-made features. Amatya [2] utilized OBIA to detect landslides along the Karnali Highway using DigitalGlobe and PlanetScope images. Object-based classification offers several advantages over conventional pixel-based classification, including the use of object shape, structure, and contextual information, resulting in clear boundaries and uniform texture. By leveraging the spatial correlation between objects, the classification process is relatively fast and efficient, achieving high accuracy with high-resolution images.

Various techniques are available for landslide susceptibility modeling, including statistical and expert system-based approaches. Recently, machine learning-based statistical methods have proven useful for spatially predicting the occurrence of landslides. Various models have been proposed for landslide susceptibility mapping (LSM) such as support vector machines (SVM) [3], [4], [5]; logistics regression (LR) [4], [6], multilayer perceptron (MLP) [7], [8], random forest (RF) [9], [10], extreme gradient boosting (XGB) [11]. These machine-learning methods have proven effective in various studies; however, some methods may outperform others in specific regions [12]. For example, Ng [13] found that RF performed better than MLP or SVM methods in predicting rainfall-induced landslides. Disagreement still exists regarding which method is the best for predicting landslide susceptibility at the local scale. Therefore, it is essential to compare and select the models with the highest performance models.

Since the training dataset may not encompass the full range of predictor characteristics present in the study area, applying the model to new regions can introduce uncertainty. To address this, Meyer & Pebesma [14] employed the Area of Applicability (AOA) approach, which defines the spatial domain where the model can be expected to capture relationships based on the training data reliably. The method is based on a Dissimilarity Index (DI), which quantifies the minimum distance between new observations and the training data in the multidimensional predictor space. The main goals of this research are to: (1) apply the OBIA to identify a landslide inventory; (2) develop a new LSM based on the most recent data and using a highly precise machine learning model and evaluate the uncertainty of LSM using the AOA approach, and (3) identify the impact of landslide conditioning factors using interpretation techniques.

2. Study area

The area is located on the western edge of the Tu Le basin, which is regarded as a continental rift [15] and lies northeast of the Song Da rift. The boundaries of these zones are marked by large faults that have reactivated during the neotectonic period, most notably the Son La fault and the Muong La –Bac Yen fault. The Tu Le basin persisted throughout the Mesozoic as an independently developed, tectonically controlled, trough-shaped basin. The lower part of the basin consists of Jurassic–Cretaceous red sediments, while the upper part comprises volcanic rocks such as rhyolite, trachyte and basalt. Intrusive magmatic rocks, including sub-alkaline and alkaline granite, gabbro, syenite, and granosyenite, constitute a small portion of the Tu Le basin.

The Pieng stream catchment, located in

Muong La commune, Son La province, is characterized by prominent geological formations of Ngoi Thia–Tu Le complex, Phu Sa Phin complex and Suoi Be formation (Fig. 1). The Tu Le–Ngoi Thia complex is divided into two volcanic sub-components: Tu Le (τλKtl), which primarily comprises trachyte, rhyolite porphyry, and trachyte porphyry; and Ngoi Thia (λτK nt), which mainly consists of rhyolite and rhyolite porphyry. The Phu Sa Phin complex (γξK pp) includes shallow and sub-volcanic intrusives such as syenite porphyr quartz and granosyenite porphyr, which are closely related in spatial distribution, formation time and origin with ryolite eruptions. The Suoi Be formation (J–K sb) mainly consists of basalt, sandstone, siltstone and tuf.

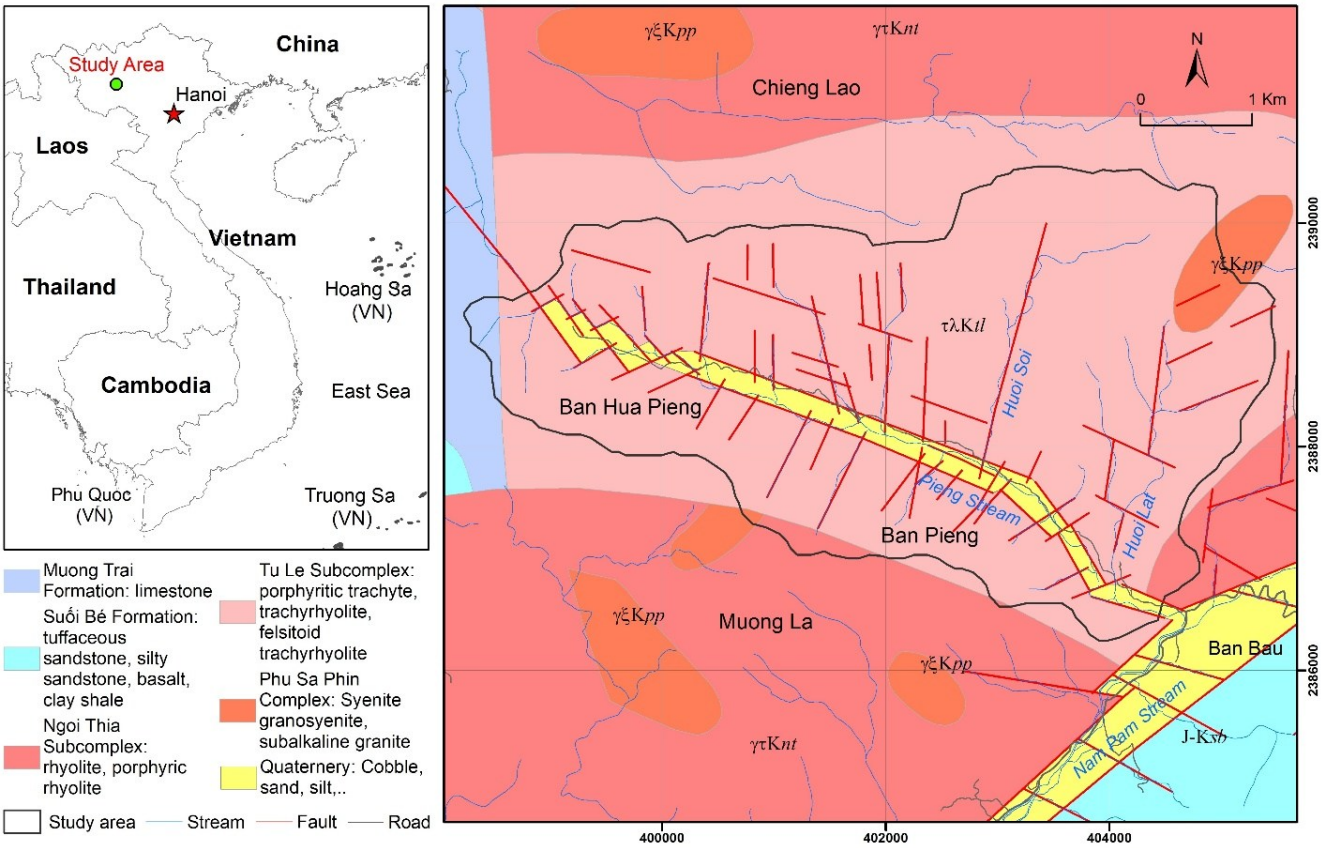

Fig. 1. Geological map of Nam Pam at a scale of 1:50.000 (modified based on [16])

The landscape of Muong La consists of steep mountain ridges rising to elevations of up to 2,469 m, trending northwest–southeast and northeast–southwest. The drainage networks on both sides of the Pieng Stream exhibit distinct characteristics. Streams on the right bank are generally shorter and steeper than those on the left, indicating a higher rate of tectonic uplift along the right side of the valley. The region's tropical climate is characterized by an annual average temperature above 22°C and a mean rainfall of roughly 1,350 mm, with the majority occurring during the May–August wet season.

3. Data preparation

PlanetScope satellite imagery (5m resolution) acquired in August 2017 was collected for OBIA. This study made use of a 5-m resolution digital elevation model (DEM) that was built by Airbus using satellite imagery data from the TanDEM-X Mission, which was mostly obtained between 2017 and 2021 [17] (Fig. 2c). From the DEM, five geomorphometric factors were derived by ArcGIS 10.8 software: aspect, curvature, relative relief, river density, slope and topographic wetness index (TWI) (Figs. 2a, 2b, 2d, 2e, 2f and 2h). The land-use and soil maps, at a scale of 1:50,000, were obtained from Son La Department of Natural Resources and Environment. The land

use map was classified into six classes, including water, natural forest, paddy land, road, annual plant, and built-up area (Fig. 2k). The soil map is divided into five classes red clay loam soil (Hs), yellowish-brown soil on mafic rocks (Fu), yellow loam soil on high mountain (A), yellow-red soil on metamorphic rocks (Fs), yellow-red soil on clay (Fl) (Fig. 2i).

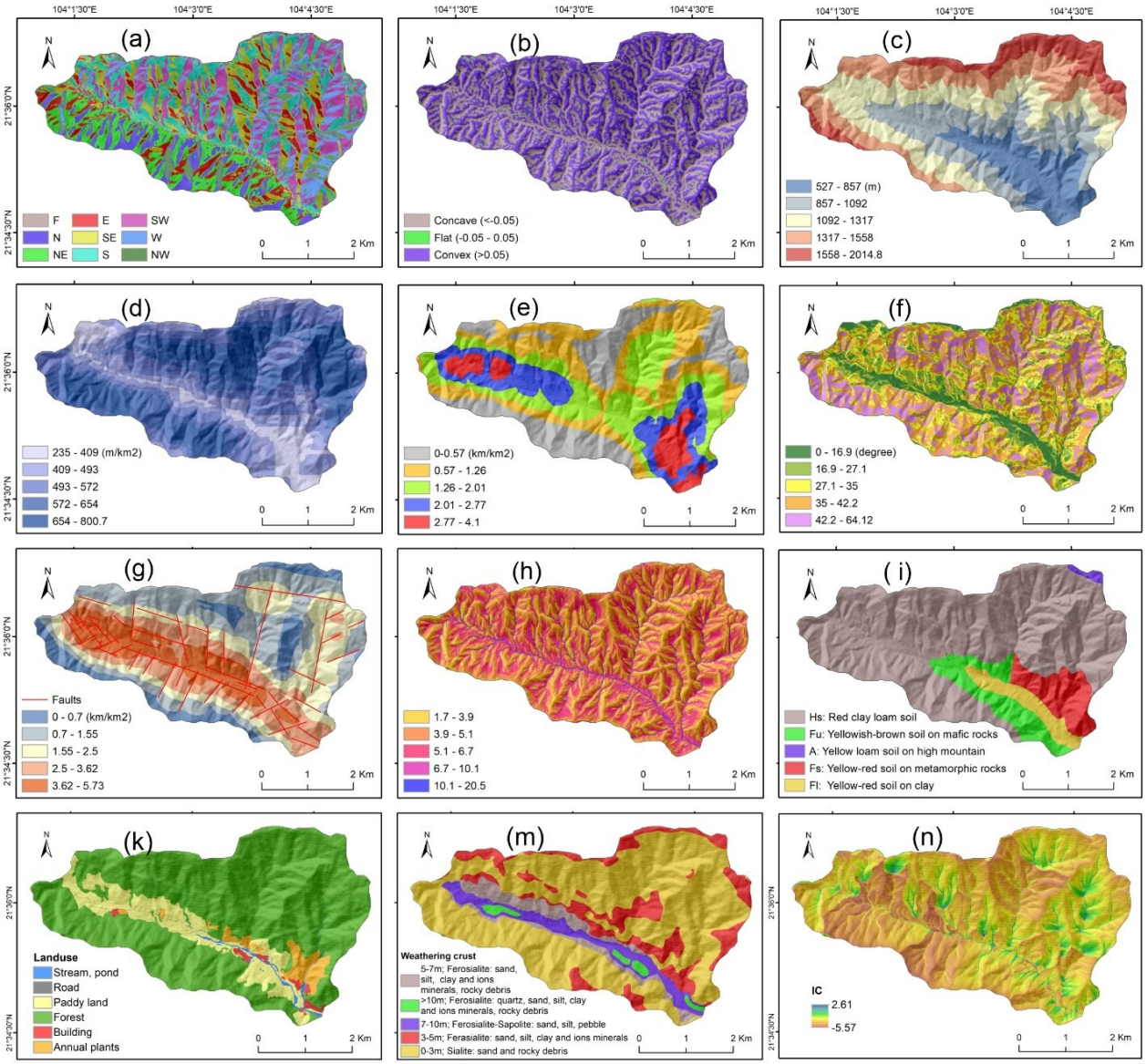

Fig. 2. Landslide explanatory variables: (a) aspect, (b) curvature, (c) elevation, (d) relative relief, (e) river density; (f) slope, (g) lineament density, (h) TWI, (i) soil; (k) landuse; (m) weathering crust and (n) index of connectivity (IC)

Lineament and weathering crust data (Figs. 2g and 2m) were supported by the national-level project "*Research using geospatial technology to assess the risk and possibility of damage due to landslides and debris flood North of Vietnam, Code: DTDL.CN-82/21*" [18]. A series of prominent lineaments with dominant NE–SW and NW–SE orientations are observed in the area. These lineaments were interpreted based on triangular tectonic facets, abrupt change in the stream system and direct indicators such as slip surfaces and scratches at the outcrop. The weathering crust map was constructed using field investigations, geomorphological analysis, geophysics and drilling data, which included four seismic lines, four resistivity lines and six boreholes. The profile is classified into five distinct classes based on depth and material composition. Class 1 (0–3 m)

corresponds to the sialite zone, consisting mainly of sand and rocky debris. Class 2 (3–5 m) is identified as ferasialite, composed of sand, silt, clay, and mineral ions. Class 3 (5–7 m) is the ferosialite layer, which includes sand, silt, clay, mineral ions, and rocky debris. Class 4 (7–10 m) represents the transition between ferosialite and saprolite, characterized by sand, silt, and pebbles. Finally, Class 5 (>10 m) represents a deep ferosialite zone containing quartz, sand, silt, clay, mineral ions, and rocky debris.

The index of connectivity (IC) is a quantitative metric used to describe landscape or sediment flow connectivity. It represents the probability that a particle released at a given point will reach the nearest sink. The IC depends on several factors, including the distance to the sink, the properties of the flow path, the amount of upslope water available for transport, and the water gained or lost along the downslope pathway. According to Borselli [19], the IC expresses the ratio between the upslope contributing area of a point and its downslope receiving area. IC values range from −∞ to +∞, where higher values indicate stronger connectivity between source areas and target sinks, while lower values reflect weaker connectivity. A DEM was utilized to develop the IC models for the study area using the SenInConnect tool [20] (Fig. 2n).

A summary of landslide predictors in terms of resolution/scale and data source is shown in Table 1.

Table 1. Data description

Factors	Resolution/Scale	Data Source
Elevation	5 m	[17]
Slope	5 m	Derived from DEM
Aspect	5 m	Derived from DEM
TWI	5 m	Derived from DEM
Curvature	5 m	Derived from DEM
Relative relief	5 m	Derived from DEM
River density	5 m	Derived from DEM
Lineament density	5 m	Field investigation
Index of connectivity	5 m	Derived from DEM
Soil	1: 10,000	Son La Natural Resources and Environment Department
Landuse	1: 10,000	Son La Natural Resources and Environment Department
Weathering crust	1: 10,000	[18]
Optical satellite image	5 m	Planet Scope

4. Methodology

4.1. Landslide inventory

The object-based image analysis (OBIA) method consists of two steps: segmentation and classification. In the segmentation step, pixels with similar brightness levels are grouped into one object. This study employs the multiresolution segmentation (MRS) method using the eCognition Developer software. The parameters of the MRS include scale, color and shape. After segmentation, objects are classified based on specific attributes and criteria, including spectral information, object size, shape features, object structure and relative location to other features [21] (Fig. 3).

To evaluate the results, some indices were calculated by overlapping areas. True positive (TP) represents the correct identification of landslides. False positives (FP) show landslides that are recognized in the image but are not in reality, whereas false negatives (FN) are actual landslides that are not recognized in the image. We divided the true positive, false positive, and false negative areas by the total observed landslide area to obtain the true positive rate (TPR), false positive rate

(FPR), and false negative rate (FNR), respectively. We also calculated the threat score (TS), which is defined as TPR divided by the sum of TPR, FPR, and FNR [22]. The detection accuracy is better when the TPR and TS values are higher. In this study, input data for OBIA include Planet Scope satellite images, DEM and its derivatives such as slope, shadow, and river.

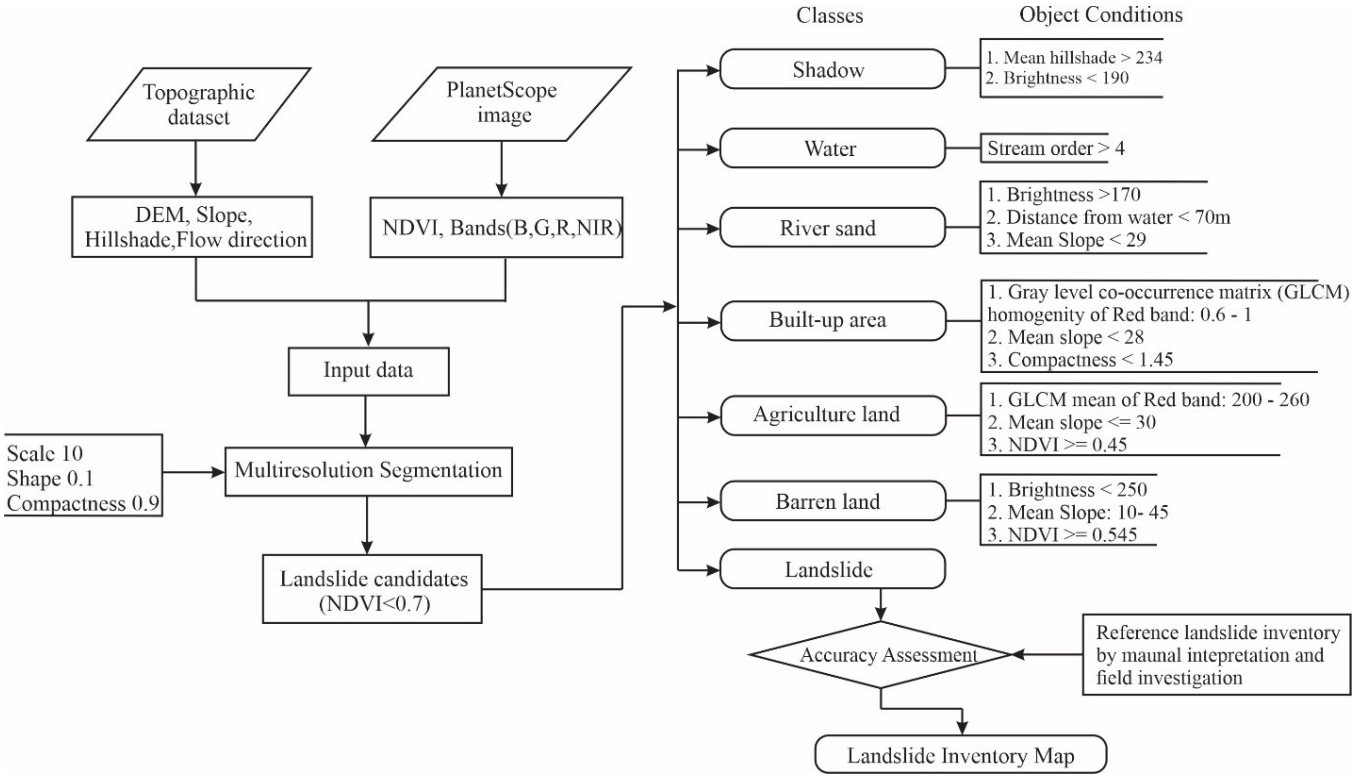

Fig. 3. Workflow chart for landslide detection (based on Martha (2011))

4.2. Modelling landslide susceptibility

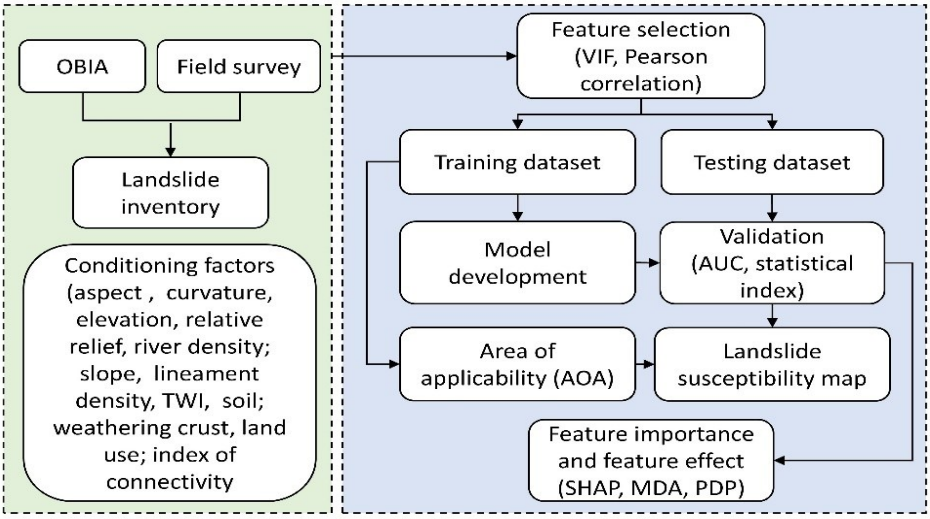

Fig. 4. Flow chart of different stages of the present study

The modeling process in this study involves several key steps, as shown in Fig. 4. First, landslide inventory data and landslide conditioning factors were collected. Next, feature selection was performed using Pearson correlation and Variance Inflation Factor (VIF) analyses to identify suitable predictors for modeling. Then, four individual models were developed and validated through ROC curves and various statistical indices, after which the landslide susceptibility map (LSM) was created based on the best-performing model. Finally, feature importance was evaluated using

Shapley Additive Explanations (SHAP) and Mean Decrease in Accuracy (MDA). In contrast, the effects of features on the model's predictions were examined using Partial Dependence Plots (PDP).

4.2.1. Preprocessing

All the landslide conditioning datasets were resampled to a spatial resolution of 5 m, with the same number of columns and rows. Because of the landslide polygons, the polygons are first gridded into points with a 5 m resolution. There is a wide range of approaches for choosing non-landslide points, such as random sampling, buffer zone method, and information value model, to identify non-landslide areas with low landslide susceptibility. The best method for selecting non-landslide points depends on the specific characteristics of the study area. In this study, non-landslide points are selected from river valleys or gentle slopes. By using this method, it is ensured that the selected non-landslide points are representative of areas with various geological and hydrological conditions. Following that, sample points were extracted and randomly divided into training datasets (70%) and testing datasets (30%).

4.2.2. Features selection

A Pearson correlation analysis was conducted for each predictor to evaluate the direction and strength of linear relationships between continuous predictor pairs. A high absolute value of correlation coefficient indicates a strong association between variables, whereas values close to zero suggest weak or no correlation. In this study, a correlation coefficient greater than 0.7 is considered indicative of significant collinearity [3]. Collinearity arises when one predictor is highly correlated with another, potentially affecting model performance and interpretability. The Variance Inflation Factor (VIF) was employed to further assess multicollinearity, a standard diagnostic tool in regression analysis. Predictors with VIF values greater than 5 were excluded [23].

4.2.3. Extreme Gradient Boosting (XGB)

In recent years, XGB has become one of the most widely used and effective techniques for scalable tree boosting [24]. XGB builds a predictive model as an ensemble of weak classification trees optimized through gradient descent with various enhancements and regularization techniques. This algorithm applies to both regression and classification tasks and is particularly efficient in reducing computational time. The parameters of XGBoost are typically categorized into three groups: general parameters, learning task parameters, and booster parameters. General parameters define the type of booster used-typically a tree-based or linear model. Learning task parameters specify the learning objective and scenario, while booster parameters are specific to the chosen booster type and control aspects such as tree depth, learning rate, and regularization.

4.2.4. Random forest (RF)

Breiman [25] first created the RF algorithm, a supervised learning technique that mixes several decision trees for enhanced performance. The basic idea of random forest is to generate a collection of uncorrelated decision trees using the bootstrap aggregation technique to create training subsets. Following the predictions made by each decision tree, the final result is either based on the average (regression) or the majority vote (classification). The training data is randomly split into subsets with replacement (bagging) for building the forest. At each node, only a random subset of the features is considered for splitting. This randomness produces stronger trees and reduces overfitting. Random Forest achieves high accuracy by reducing variance, is less prone to overfitting than single decision trees, and can handles both classification and regression tasks.

4.2.5. Multi-layer perceptron (MLP)

MLP is an artificial neural network composed of input, hidden, and output layers. Hidden layers use activation functions to process input data and pass the information to the output layers. Nodes in each layer are connected to the subsequent layer, with a non-linear activation function for each

hidden layer node [26]. Layers are linked by weights and optimized through a process called backpropagation. This process involves calculating the error, using gradient descent to update the weights, and repeating the process until the error falls within an acceptable range. To model the landslides susceptibility, this study chose MLP as the basis classifier with hyper-parameter settings.

4.2.6. Logistic regression (LR)

LR is a statistical model that uses a sigmoid function to predict the probability of a binary outcome (landslide or non-landslide) based on a set of predictor variables [27]. It is also possible to assess the degree of association between the independent and dependent variables by utilizing the odds ratio calculated by logistic regression. As a result, this method has found widespread application in landslide susceptibility studies.

4.2.7. Hyperparameters tuning and validation criteria

Grid search combined with 10-fold cross-validation (k = 10) was employed to determine the optimal hyperparameters for each model using the training dataset. Model performance on the validation set was evaluated using accuracy as the scoring metric. For the Random Forest (RF) model, three parameters were tuned: n_estimators (the number of trees in the forest), max_features (the maximum number of features considered when splitting a node), and max_depth (the maximum depth of each decision tree). For the Logistic Regression (LR) model, the tuning focused on C (the regularization strength) and max_iter (the maximum number of iterations). In the case of the XGBoost (XGB) model, three general parameters were adjusted: max_depth (the maximum depth of a tree), learning_rate (the step size shrinkage to prevent overfitting), and subsample (the fraction of training instances used for each iteration). Finally, for the Multilayer Perceptron (MLP) classifier, several parameters were optimized, including hidden_layer_sizes, activation function, and learning_rate.

A well-liked method for assessing how well models perform on datasets is the receiver operating characteristic (ROC) curve. In addition, the effectiveness of the landslide prediction models was evaluated using some statistical indices, including accuracy, precision, recall, F1 score and kappa index [4].

4.3. Feature importance and feature effect

Three interpretability techniques, i.e., SHAP, MDA, and PDP, were applied to better understand the role of each conditioning factor. SHAP values were employed to identify the most influential landslide conditioning factors and assess their relative importance. Based on game theory, SHAP assigns an importance score to each feature, where higher SHAP values indicate a greater impact on model predictions [28]. In addition to SHAP, feature importance was evaluated using the mean decrease in accuracy (MDA) method. MDA quantifies the drop in model accuracy when a specific feature is permuted; a larger decrease in accuracy signifies higher feature importance [29].

A partial dependence plot (PDP) is a useful tool for interpreting the relationship between individual features and the predicted output of a machine learning model [30]. The PDP is generated by replicating the dataset m times, where m represents the number of unique values in the feature of interest while keeping all other features constant. The model's average prediction is calculated for each unique value of the target feature, illustrating how variations in that feature affect the model's output.

5. Results and discussion

5.1. Landslide detection

The landslide inventory results are based on a combination of OBIA and field surveys conducted during the period 2017–2023 are presented in Fig. 6, showing a total of 98 mapped landslides (Fig. 5). The analysis yielded the following accuracy metrics: TP (66,121 m^2), FP (36,023 m^2), FN (7,662 m^2), TPR (0.896) and TS (0.602). The results demonstrate a level of reliability comparable to previous studies, such as TPR = 0.6, TS = 0.44 [22]. There are various types of landslides in the

area, including rotational earth slides, debris slides, and debris flows of varying scales (Fig. 6). The large landslides are distributed along both sides of the Pieng stream valley, extending in the NW-SE direction. Based on the landslide classification by area (m²) proposed by Cornforth [31], the Nam Pam region contains 8 large landslides (20,000–200,000 m²), 43 medium landslides (2,000–20,000 m²), and 47 small landslides (200–2,000 m²).

Several issues remain in OBIA classification. Because each object is optimally represented only at a specific scale, a single scale value cannot adequately capture all object sizes. To address this problem, it is necessary to select an appropriate scale for object-based classification. Several methods have been proposed for the automatic determination of optimal scale, such as the Estimation of Scale Parameter 2 [32] or Plateau Objective Function [33]. However, no study has yet confirmed a universally optimal scale value. Another main limitation of OBIA is the difficulty in detecting ancient or potential landslides obscured by vegetation cover. This limitation highlights the importance of acquiring remote sensing images as soon as possible after landslide events and conducting field surveys to build a comprehensive and accurate landslide inventory.

This study represents the first application of the OBIA method for landslide inventory mapping, particularly for a mountainous catchment in Vietnam. Compared to conventional pixel-based classification or manual digitization, this object-based approach enables a more refined delineation of landslide features by integrating spectral and spatial information. The OBIA is well-suited for high-resolution satellite imagery (e.g., Planet Scope 5m) and is highly applicable in mountainous regions where landslide scars are often small, irregularly shaped, and mixed with other land cover types. In regions with sparse and limited field-based inventories, the OBIA method can provide a semi-automated approach to generate accurate landslide data, which are essential for model training and hazard mapping.

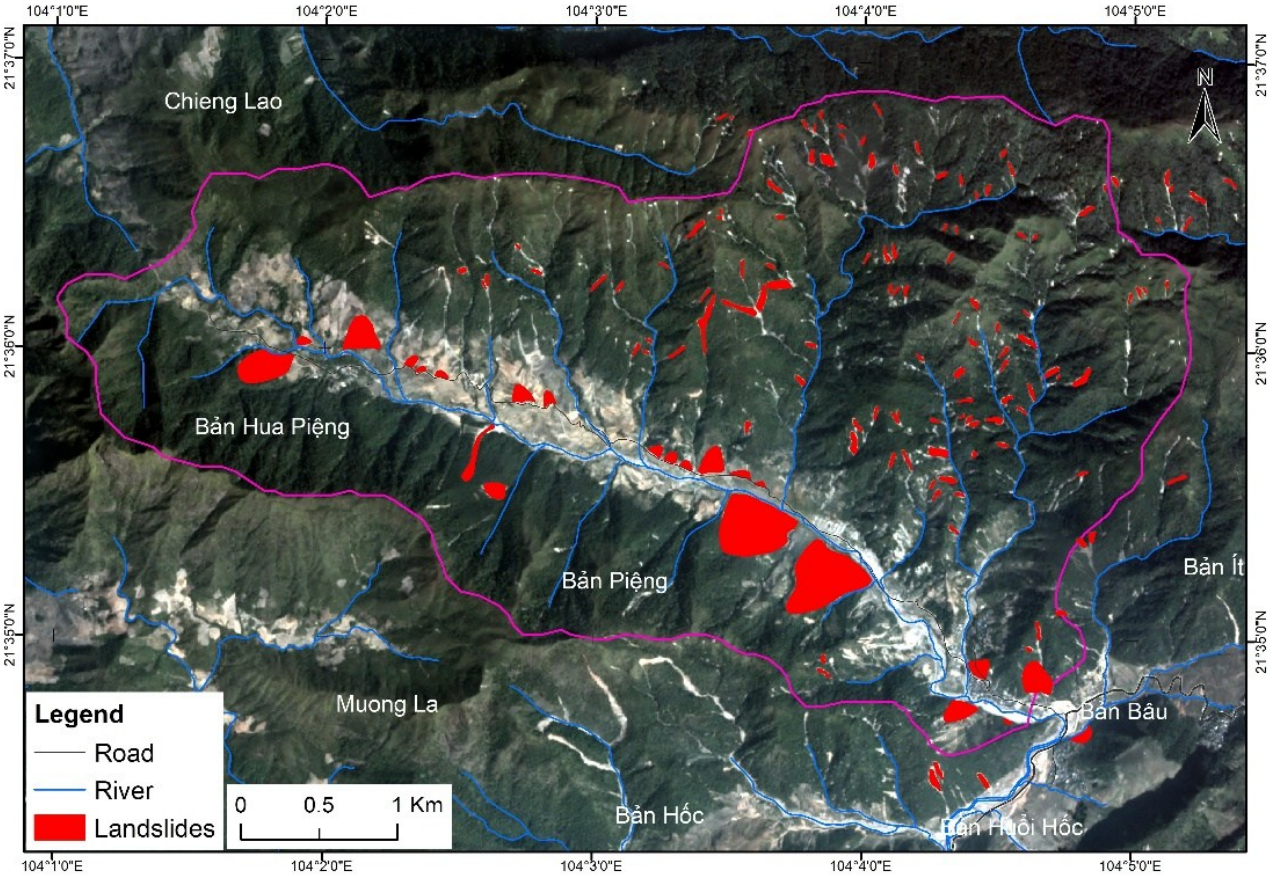

Fig. 5. Landslide inventory map using OBIA and field survey

Fig. 6. Landslides in Nam Pam: The landslide in Ban Pieng in July 2022 caused soil cracking and cracks in the walls of local houses (A), (B), (C), and (D); and landslide displaced the road in Ban Pieng (E) and (F)

5.2. Model validation and landslide susceptibility mapping

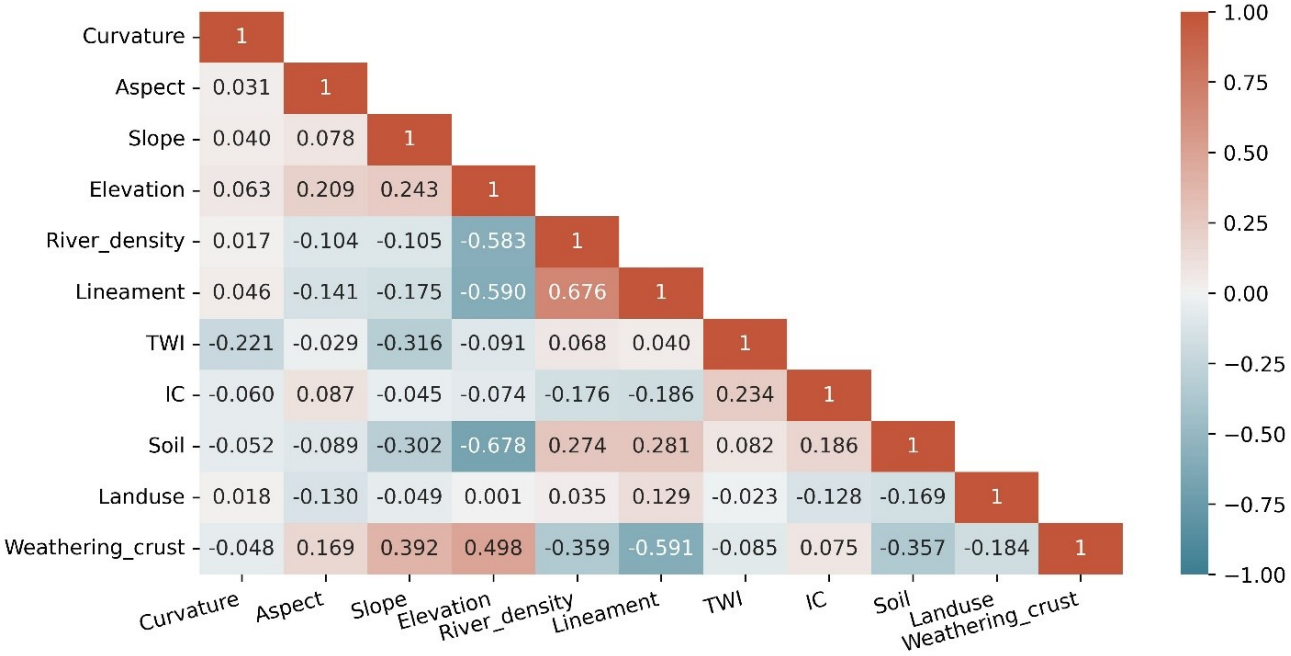

Fig. 7. Pearson correlation coefficient between pairs of landslide influencing factors

Table 2. VIF and TOL values of landslide conditioning factors

Predictors	VIF	TOL
Curvature	1.073	0.932
Aspect	1.125	0.889
Slope	1.445	0.692
Elevation	3.299	0.303
Relative relief	1.883	0.531
River density	2.388	0.419
Lineament	2.715	0.368
TWI	1.256	0.796
IC	1.246	0.803
Soil	2.382	0.420
Landuse	1.134	0.882
Weathering crust	2.076	0.482

From the identified landslide polygons, 570 landslide points were extracted and used for model training. To ensure an equal number of landslide and nonlandslide points, a total of 570 non-landslide points were generated. All predictors exhibited VIF values below 5 (Table 2), and the Pearson correlation coefficients were all less than 0.7 (Fig. 7), indicating low multicollinearity and weak correlations among variables [10]. Consequently, eleven landslide conditioning factors were retained for modelling.

Table 3 and Fig. 8 present the model validation results, highlighting the XGB model as the most accurate for both the training and testing datasets. During the training phase, the XGB model outperformed the others across most evaluation metrics, achieving high precision (0.962), recall (0.957), accuracy (0.96), F1 score (0.96), and kappa (0.92) (Table 3). Additionally, a high AUC value of 0.985 further confirms the strong performance of the XGB model (Fig. 8). Similar trends were observed in the testing phase, where the XGB model again demonstrated superior performance with precision (0.913), recall (0.918), accuracy (0.915), F1 score (0.915), kappa (0.83), and AUC (0.961). XGB yielded the best performance, confirming its capability to model nonlinear dependencies among the input variables. This finding is consistent with previous research on landslide susceptibility [11, 34].

After applying the XGB model to the entire study area, we could obtain an LSM. The area of applicability (AOA) analysis confirmed that the XGB model is generally applicable throughout the study area, with only minor zones of inapplicability observed along the main streams (Fig. 9). Areas outside the AOA covered merely 0.79% of the study region, indicating a high level of model applicability. LSM is divided into five susceptibility categories by the natural break method: very low, low, moderate, high, and very high classes of susceptibility (Fig. 9). These classes covered 33.64%, 15.78%, 12.35%, 15.41 %, and 22.82%, respectively, of the area satisfying the AOA. Landslide points from the testing data are overlaid on the predictive map to confirm the accuracy of the LSM. With very high (3.27) and high (0.88) frequency ratio values, we found that most of the testing data landslides are classified as very high and high (>88%) (Fig. 10). This finding demonstrates the high accuracy of the LSM. To assess the performance of the proposed model, we compared it with previous research. Quan [35] produced a 10-m resolution LSM for the Nam Pam catchment using 5,946 landslide pixels and an ensemble of LADT combined with bagging, dagging, and multiboosting, achieving an AUC of 0.9. The results indicate that the XGB model used in this study provides more effective landslide prediction.

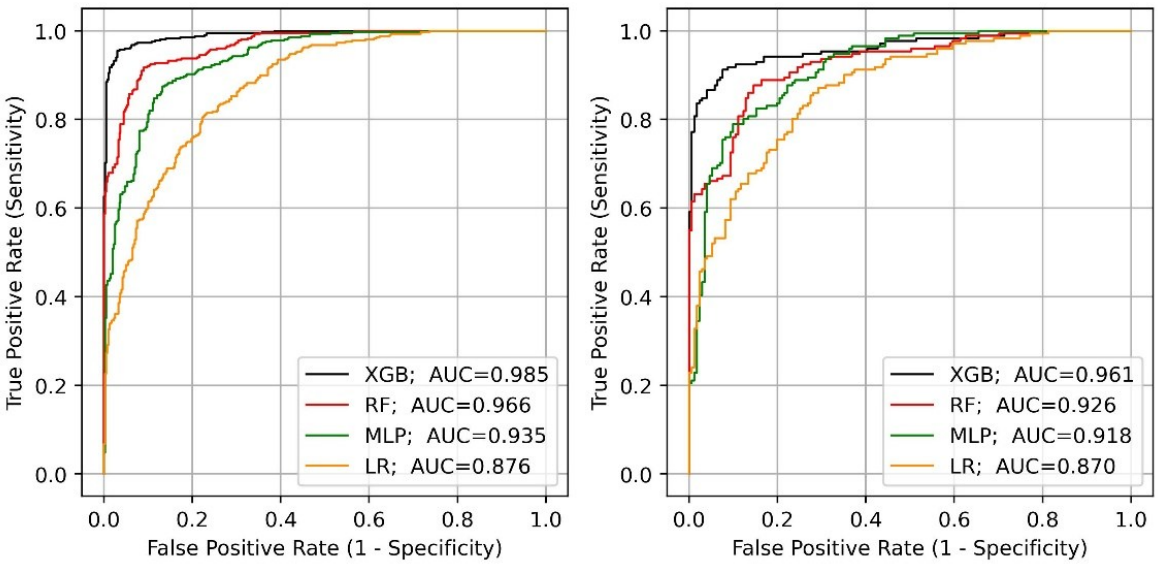

Fig. 8. Comparison of different model using ROC curve (a) training dataset (b) testing dataset

Table 3. Statistical indices of training dataset and testing dataset

Dataset	Model	Precision	Recall	ACC	F1-score	kappa
Training Set	XGB	0.962	0.957	0.960	0.960	0.920
	RF	0.912	0.910	0.911	0.911	0.822
	MLP	0.905	0.762	0.841	0.827	0.682
	LR	0.788	0.762	0.778	0.775	0.556
Testing Set	XGB	0.913	0.918	0.915	0.915	0.830
	RF	0.844	0.889	0.863	0.866	0.725
	MLP	0.897	0.760	0.836	0.823	0.673
	LR	0.791	0.754	0.778	0.772	0.556

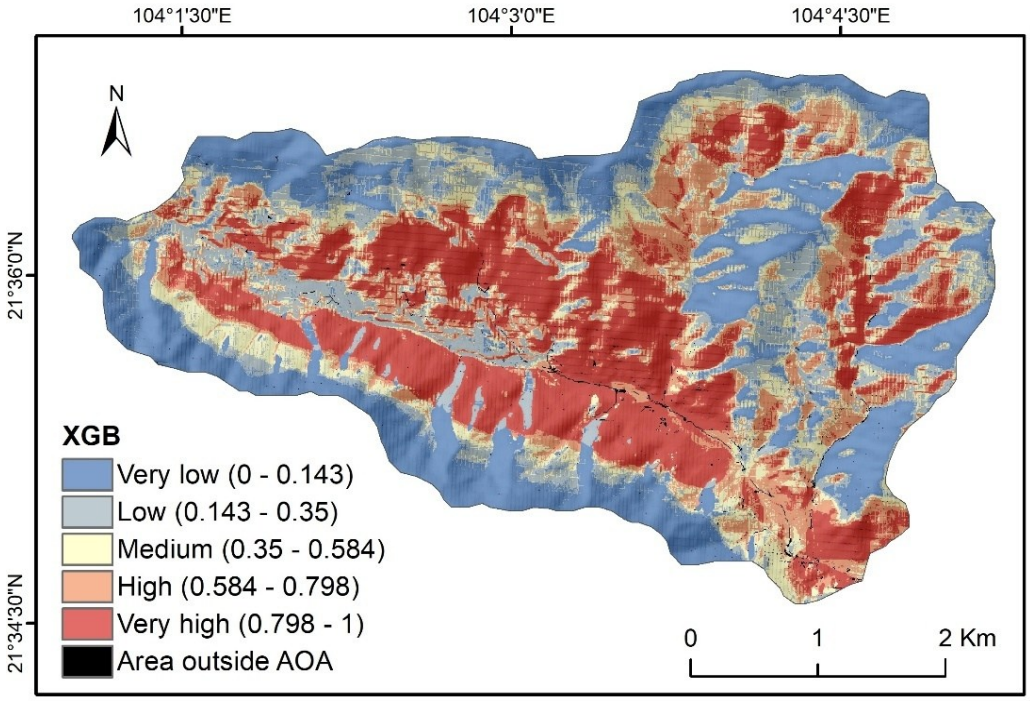

Fig. 9. Landslide susceptibility map of Nam Pam using XGB model

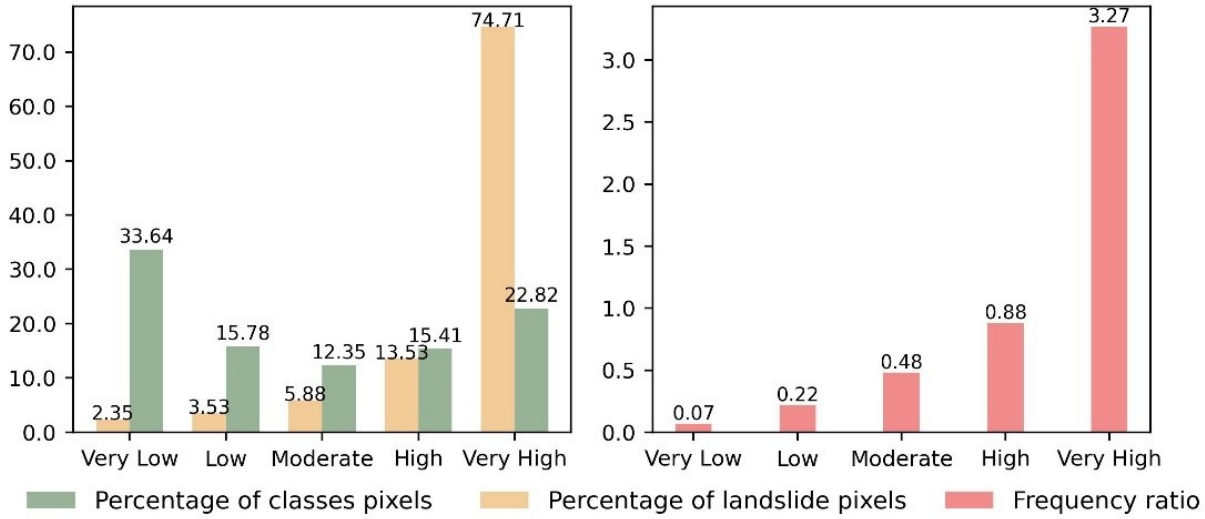

Fig. 10. Analysis of landslide density on the susceptibility map using XGB model

In recent decades, landslides have occurred with increasing frequency during the rainy and stormy seasons, causing severe losses of life and property in Vietnam [36], [37], [38], [39]. Landslide hazard mapping has been conducted in numerous mountainous regions. However, most previous studies developed landslide susceptibility maps at the provincial or district level with smaller scales, such as 1:50,000 or 1:25,000. The current research successfully constructed a large-scale susceptibility map at the catchment level for the Pieng stream area. Significantly, we utilized a 5 m high-resolution DEM generated by Airbus from TanDEM-X satellite imagery, providing significantly finer topographic detail compared to previous studies in Vietnam. The use of this high-resolution DEM improves the accuracy and reliability of our catchment-scale susceptibility mapping, especially in the complex and rugged terrain of Northern Vietnam. As a result, our mapping more precisely captures the topographic controls on landslide occurrence, supporting a robust assessment of susceptibility at the catchment scale. Furthermore, the study results demonstrate that combining machine learning with AI techniques can improve predictive accuracy and provide a feasible framework for large-scale, data-driven mapping in other vulnerable catchments across the Northern mountainous region. The LSM, therefore, enables more accurate localization of landslide-prone areas, which is crucial for disaster preparedness, local risk management, and land-use planning. The detailed susceptibility information is especially useful for village- or commune-level disaster risk reduction planning, such as relocation planning or installation of early warning systems.

5.3. Feature importance and feature effect

A comprehensive evaluation of variable importance and their influence on landslide probability was performed using the multi-faceted approach of SHAP, MDA and PDP. Features with positive SHAP values have a positive impact on the prediction, while those with negative values have a negative impact. The SHAP values for the 12 features used are displayed in Fig. 11. The results indicate that lineament density and aspect had the greatest impact on the landslide susceptibility model, followed by river density, slope and elevation. In addition, the similarity between the SHAP and MDA plots demonstrates the robustness of the XGB model in landslide prediction.

Fig. 12 presents the landslide probability variation of predictors using the XGB model. Landslide susceptibility increases with increasing slope, relative relief, lineament density, river density and aspect (0-150^0). The analysis revealed a non-linear relationship between elevation and landslide probability. The study area is located in a highly mountainous region with complex topography and steep elevation gradients due to

high relative relief. This pattern likely reflects the interaction between topographic and climatic factors. Higher elevations generally increase exposure to intense rainfall events. High terrain may coincide with zones of tectonic uplift or active deformation, exacerbating rock's long-term weakening and weathering. Areas with high relative relief tend to have steep, dissected slopes, where gravitational mass movements are more likely to occur. In addition, the Nam Pam area is characterized by high lineament and river densities, which are typically associated with fractured zones in one of the most tectonically active regions of Northwestern Vietnam. The tectonic discontinuities weaken rock masses, forming pathways for water infiltration deeply into the slope and exacerbating slope failures. Therefore, high lineament density presents one of the significant contributing factors to landslides in the study area.

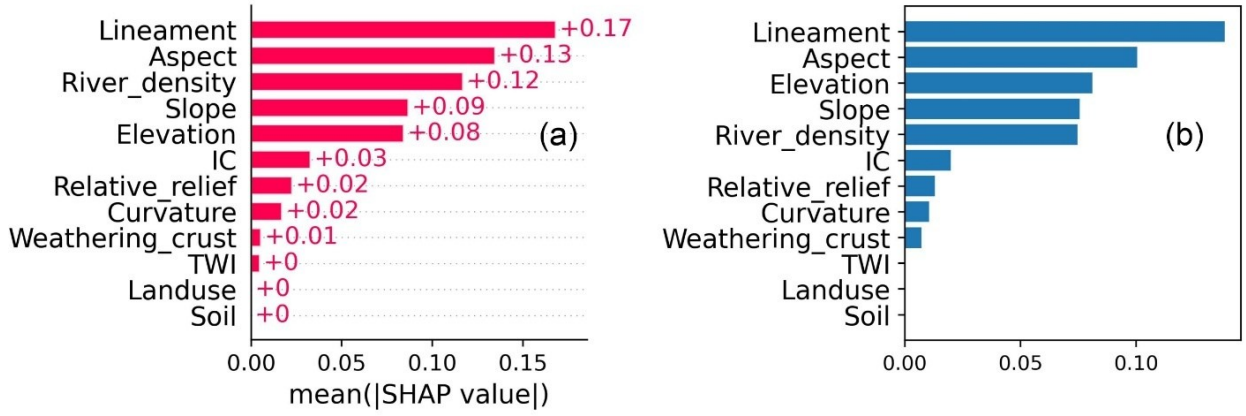

Fig. 11. Feature ranking by SHAP (a) and MDA (b).

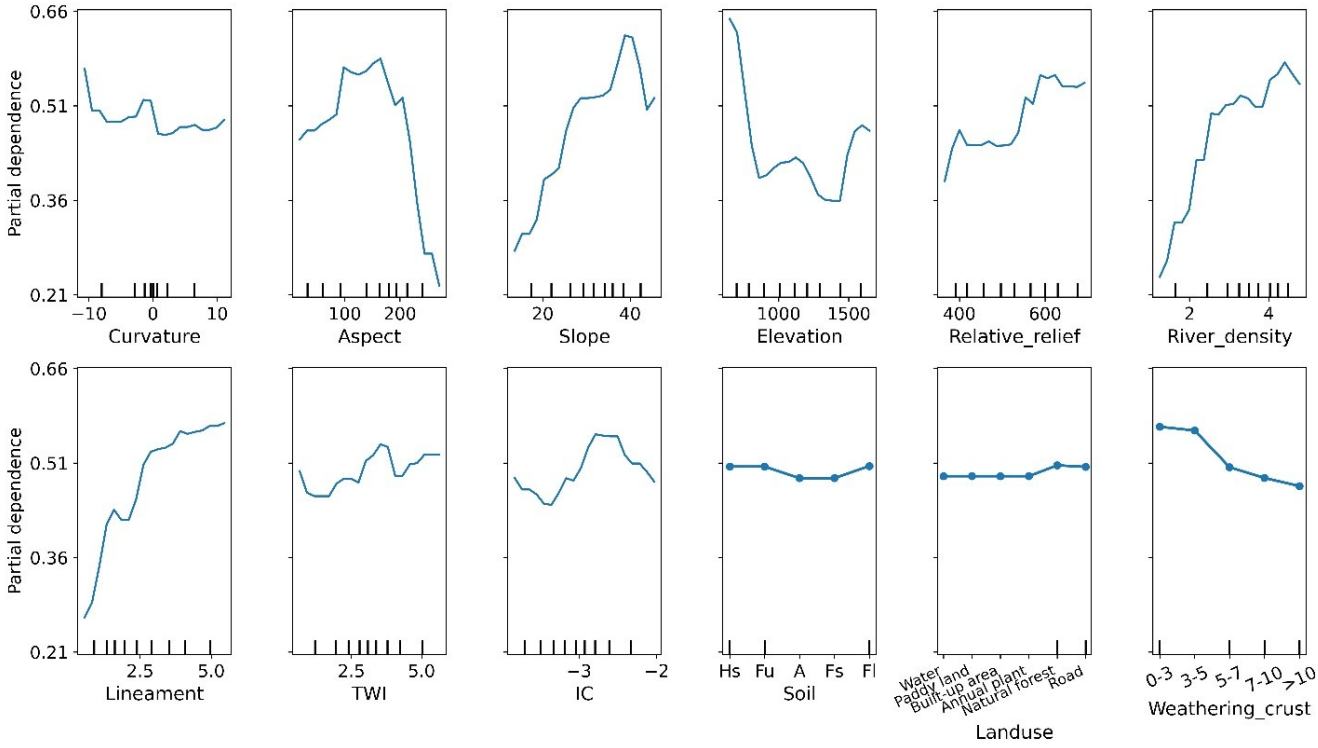

Fig. 12. PDP of the selected predictors

In addition, soil, land-use and weathering crust were the categorical variables in the model. Both soil and land use have a similar influence on landslides. In contrast, areas with a weathering crust thickness of less than 5m exhibit a higher probability of landslide occurrence. The influence

of topographic wetness index (TWI) and aspect also reveals the importance of hydrological accumulation and slope orientation in controlling moisture distribution, a key trigger in rainfall-induced landslides.

6. Conclusions

The Nam Pam catchment has been considered a highly vulnerable area to devastating landslide disasters in Northern Vietnam. The study results demonstrated a high level of reliability for the OBIA method for landslide detection, with a TPR of 0.886 and a TS of 0.602. Among the tested models for landslide susceptibility analysis, the XGB model showed the best performance, achieving an AUC of 0.961, an F1 score of 0.915, and an accuracy of 0.915 on the testing dataset. Additionally, the results using SHAP values also indicate that lineament and aspect are the major contributing factors to landslide susceptibility in the study area. Landslide susceptibility increases with increasing slope, relative relief, lineament density, river density and aspect ($0\text{-}150^0$).

This study demonstrates the effectiveness of integrating Object-Based Image Analysis (OBIA) with machine learning algorithms for landslide susceptibility assessment. The results confirm the potential of OBIA for developing detailed and accurate landslide inventories from high-resolution imagery, especially in areas where landslide scars are small or covered by vegetation. The proposed framework offers a replicable approach for catchment-scale susceptibility mapping and can be applied to larger mountainous regions in Vietnam to support disaster risk reduction, land-use planning, and early warning systems. However, several limitations should be noted. The study relied on a limited number of landslide points, did not explicitly consider rainfall as a triggering factor, and did not include deep learning approaches, which may further improve predictive performance. Future research should address these aspects to enhance the robustness and general applicability of the proposed framework.

Funding

This research was financially supported by the Vietnam Academy of Science and Technology (VAST) under Project Code CT0649.01/21-23.

Data availability statement

The data utilized in this study are available from corresponding authors upon a reasonable request.

Conflicts of interest

The authors declare no conflict of interest.

References

[1] J. Barlow, Y. Martin, S. Franklin. (2003). Detecting translational landslide scars using segmentation of Landsat ETM+ and DEM data in the northern Cascade Mountains, British Columbia. *Canadian Journal of Remote Sensing*, 29(4), 510-517. https://doi.org/10.5589/m03-018

[2] P.M. Amatya, D. Kirschbaum, T. Stanley. (2019). Use of Very High-Resolution Optical Data for Landslide Mapping and Susceptibility Analysis along the Karnali Highway, Nepal. *Remote Sensing*, 11, 2284. https://doi.org/10.3390/rs11192284

[3] B.T. Dieu, T.A. Tuan, H. Klempe, B. Pradhan, I. Revhaug. (2016). Spatial prediction models for shallow landslide hazards: a comparative assessment of the efficacy of support vector machines, artificial neural networks, kernel logistic regression, and logistic model tree. *Landslides*, 13, 361–378. https://doi.org/10.1007/s10346-015-0557-6

[4] T.V. Phong, T.T. Phan, I. Prakash, S.K. Singh, A. Shirzadi, K. Chapi, H.-B. Ly, L.S. Ho, N.K. Quoc, B.T. Pham. (2019). Landslide susceptibility modeling using different artificial intelligence methods: a case study at Muong Lay district, Vietnam. *Geocarto International*, 36, 1685. https://doi.org/10.1080/10106049.2019.1665715.

[5] T. Tuan, P. Pha, T. Tam, D. Bui. (2023). A New Approach Based on Balancing Composite Motion Optimization and Deep Neural Networks for Spatial Prediction of Landslides at

Tropical Cyclone Areas. *IEEE Access*, 11, 69495-69511. https://doi.org/10.1109/ACCESS.2023.3291411

[6] B.T. Dieu, O. Löfman, I. Revhaug, Ø. Dick. (2011). Landslide susceptibility analysis in the Hoa Binh province of Vietnam using statistical index and logistic regression. *Natural Hazards*, 59, 1413–1444. https://doi.org/10.1007/s11069-011-9844-2

[7] N.D. Dam, H.V. Le, B.T. Pham. (2023). Landslide susceptibility modeling and mapping at Dien Bien province, Vietnam using Bagging based MLP neural network. *IOP Conference Series: Materials Science and Engineering*, 1289, 012020. https://doi.org/10.1088/1757-899X/1289/1/012020

[8] B.D. Quynh, H. Ha, K. Dong, J. von Meding, L. Nguyen, C. Luu. (2022). Landslide susceptibility prediction mapping with advanced ensemble models: Son La province, Vietnam. *Natural Hazards*, 116, 2283–2309. https://doi.org/10.21203/rs.3.rs-1650275/v1

[9] T.X. Bien, M. Iqbal, A. Jamal, D.D. Nguyen, T.V. Phong, R. Costache, L.S. Ho, H.V. Le, H.B.T. Nguyen, I. Prakash, B.T. Pham. (2023). Integration of rotation forest and multiboost ensemble methods with forest by penalizing attributes for spatial prediction of landslide susceptible areas. *Stochastic Environmental Research and Risk Assessment*, 37, 4641–4660. https://doi.org/10.1007/s00477-023-02521-1

[10] B.T. Pham, T.V. Phong, T. Nguyen-Thoi, P.T. Trinh, Q.C. Tran, L.S. Ho, S.K. Singh, T.T.T. Duyen, L.T. Nguyen, H.Q. Le, H.V. Le, N.T.B. Hanh, N.K. Quoc, I. Prakash. (2020). GIS-based ensemble soft computing models for landslide susceptibility mapping. *Advances in Space Research*, 66(6), 1303-1320. https://doi.org/10.1016/j.asr.2020.05.016

[11] H. Ha, Q.D. Bui, D.T. Tran, D.Q. Nguyen, H.X. Bui, C. Luu. (2024). Improving the forecast performance of landslide susceptibility mapping by using ensemble gradient boosting algorithms. *Environment, Development and Sustainability*, 27, 18409–18443. https://doi.org/10.1007/s10668-024-04694-3

[12] A.M. Youssef, H.R. Pourghasemi. (2021). Landslide susceptibility mapping using machine learning algorithms and comparison of their performance at Abha Basin, Asir Region, Saudi Arabia. *Geoscience Frontiers*, 12, 639–655. https://doi.org/10.1016/j.gsf.2020.05.010

[13] C.W.W. Ng, B. Yang, Z.Q. Liu, J.S.H. Kwan, L. Chen. (2021). Spatiotemporal modelling of rainfall-induced landslides using machine learning. *Landslides*, 18, 2499–2514. https://doi.org/10.1007/s10346-021-01662-0.

[14] H. Meyer, E. Pebesma. (2021). Predicting into unknown space? Estimating the area of applicability of spatial prediction models. *Methods in Ecology and Evolution*, 12(1), 1-21. https://doi.org/10.1111/2041-210X.13650

[15] D.L. Tran, X.B. Nguyen. (1988). Geological map of Viet Nam scale 1:500,000.

[16] N. Vinh, D.K. Thuy, N.C. Luong, P.T. Thi. (2005). Geological and resources map of Yen Bai at a scale of 1: 200,000.

[17] D.D. Cham. (2024). Field reports and Digital Elevation Model data. Project code CT0649.01/21-23, Vietnam Academy of Science and Technology.

[18] N.C. Quan. (2025). Field reports and Digital Elevation Model data. Project code DTDL.CN-82/21, Vietnam Ministry of Science and Technology.

[19] L. Borselli, P. Cassi, D. Torri. (2008). Prolegomena to sediment and flow connectivity in the landscape: A GIS and field numerical assessment. *CATENA*, 75, 268–277. https://doi.org/10.1016/j.catena.2008.07.006

[20] S. Crema, M. Cavalli. (2018). SedInConnect: a stand-alone, free and open source tool for the assessment of sediment connectivity. *Computers & Geosciences*, 111, 39–45. https://doi.org/10.1016/j.cageo.2017.10.009

[21] T.R. Martha. (2011). Detection of landslides by

objectoriented image analysis. Degree of doctor, University of Twente.

[22] E. Bessette-Kirton, J. Kean, J. Coe, F. Rengers, D. Staley. (2019). An evaluation of debris-flow runout model accuracy and complexity in Montecito, California: Towards a framework for regional inundation-hazard forecasting. *The 7th International Conference on Debris-Flow Hazards Mitigation*, pp. 257-264.

[23] D.W. Hosmer, S. Lemeshow, R.X. Sturdivant. (2013). Applied Logistic Regression 3rd Edition. John Wiley & Sons. https://doi.org/10.1002/9781118548387

[24] T. Chen, C. Guestrin. (2016). XGBoost: A Scalable Tree Boosting System. KDD '16: Proceedings of the 22nd ACM SIGKDD International Conference on Knowledge Discovery and Data Mining, pp. 785–794. https://doi.org/10.1145/2939672.2939785

[25] L. Breiman. (2001). Random Forests. *Machine Learning*, 45, 5–32. https://doi.org/10.1023/A:1010933404324

[26] D. Li, F. Huang, L. Yan, Z. Cao, J. Chen, Z. Ye. (2019). Landslide Susceptibility Prediction Using Particle-Swarm-Optimized Multilayer Perceptron: Comparisons with Multilayer-Perceptron-Only, BP Neural Network, and Information Value Models. *Applied Sciences*, 9, 3664. https://doi.org/10.3390/app9183664

[27] N. Regmi, R. Giardino, E. Mcdonald, J. Vitek. (2013). A comparison of logistic regression-based models of susceptibility to landslides in western Colorado, USA. *Landslides*, 11, 247–262. https://doi.org/10.1007/s10346-012-0380-2

[28] S.M. Lundberg, S.I. Lee. (2017). A Unified Approach to Interpreting Model Predictions. *NIPS'17: Proceedings of the 31st International Conference on Neural Information Processing Systems*, *pp. 4768-4777.* https://doi.org/10.48550/arXiv.1705.07874

[29] R. Das, P.V. Tien, K.W. Wegmann, M. Chakraborty. (2024). Machine learning-based assessment of regional-scale variation of landslide susceptibility in central Vietnam. *PLOS ONE*, 19, e0308494. https://doi.org/10.1371/journal.pone.0308494

[30] J.H. Friedman. (2001). Greedy function approximation: A gradient boosting machine. *The Annals of Statistics*, 29, 1189–1232. https://doi.org/10.1214/aos/1013203451

[31] D. Cornforth. (2005). Landslides in Practice: Investigation, Analysis, and Remedial/ Preventative Options in Soils. John Wiley & Sons.

[32] L. Drăguţ, O. Csillik, C. Eisank, D. Tiede. (2014). Automated parameterisation for multi-scale image segmentation on multiple layers. *ISPRS Journal of Photogrammetry and Remote Sensing*, 88, 119–127. https://doi.org/10.1016/j.isprsjprs.2013.11.018

[33] T. Martha, N. Kerle, C.J. Westen, V.G. Jetten, K. vinod Kumar. (2012). Object-oriented analysis of multi-temporal panchromatic images for creation of historical landslide inventories. *ISPRS Journal of Photogrammetry and Remote Sensing*, 67, 105–119. https://doi.org/10.1016/j.isprsjprs.2011.11.004

[34] A. Zhang, X. Zhao, X. Zhao, X. Zheng, M. Zeng, X. Huang, P. Wu, T. Jiang, S. Wang, J. He, Y. Li. (2024). Comparative study of different machine learning models in landslide susceptibility assessment: A case study of Conghua District, Guangzhou, China. *China Geology*, 7, 104–115. https://doi.org/10.31035/cg2023056

[35] C.Q. Nguyen, D.A. Nguyen, H.T. Tran, T.T. Nguyen, B.T.P. Thao, N.T. Cong, T.V. Phong, H.V. Le, I. Prakash, B.T. Pham. (2025). Predicting landslide and debris flow susceptibility using Logitboost alternating decision trees and ensemble techniques. *Natural Hazards*, 121, 1661–1686. https://doi.org/10.1007/s11069-024-06844-2

[36] L.H. Luong, T. Miyagi, P.V. Tien, D.H. Loi, H. Eisaku, S. Abe. (2017). Landslide Risk Evaluation in Central Provinces of Vietnam.

Advancing Culture of Living with Landslides, pp. 1145–1153. WLF 2017. Springer, Cham. https://doi.org/10.1007/978-3-319-534985_130

[37] P.V. Tien, P.T. Trinh, L.H. Luong, L.M. Nhat, D.M. Duc, T.T. Hieu, T.Q. Cuong, T.T. Nhan. (2021). The October 13, 2020, deadly rapid landslide triggered by heavy rainfall in Phong Dien, Thua Thien Hue, Vietnam. *Landslides*, 18, 2329–2333. https://doi.org/10.1007/s10346-021-01663-z.

[38] P.V. Tien, L.L. Hong, N.T. Thanh, P.N. Quoc, T.P. Trong, Q.D. Thi, D.D. Minh, L.N. Chau, C.N. Hai. (2023). Mechanism and numerical simulation of a rapid deep-seated landslide in Van Hoi reservoir, Vietnam. *Vietnam Journal of Earth Sciences*, 45, 357–373. https://doi.org/10.15625/2615-9783/18539

[39] P.V. Tien, V.C. Minh, D.M. Duc, L.H. Luong, D.H. Nam, T.T. Hieu. (2025). Rainfall-induced catastrophic rapid and long-traveling landslide in Lang Nu hamlet: the worst natural landslide disaster in Vietnam. *Landslides*, 22, 1761–1767. https://doi.org/10.1007/s10346-025-02490-2